International Journal of Pharmaceutics 671 (2025) 125298

Contents lists available at ScienceDirect

International Journal of Pharmaceutics

journal homepage: www.elsevier.com/locate/ijpharm

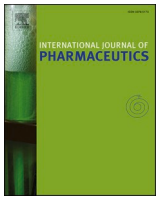

DSP_{index} guides dose selection to extend drug supersaturation lifetime during cocrystal dissolution

Lucy M. Newman, Oisín N. Kavanagh, Tatiane C. Machado *

School of Pharmacy, Newcastle University, United Kingdom

ARTICLE INFO

Keywords:
Cocrystal solubility
Critical supersaturation
Coformer concentration
Drug precipitation
Solution-mediated phase transformation

ABSTRACT

Synchronising both cocrystal dissolution and drug precipitation processes is the key for the development of cocrystal systems with desired dissolution-supersaturation-precipitation (DSP) behaviours. Our findings with ketoconazole (KTZ) – *p*-aminobenzoic acid (PABA) 1:1 cocrystal show that this can be achieved by generating non-stoichiometric coformer concentrations that allow us to modulate the maximum theoretical cocrystal supersaturation SA (thermodynamic limit) below the drug critical supersaturation σ_{crit} (kinetic limit). The application of our conceptual graphical approach combined with the two metrics SA and the DSP_{index} answer the question of how much additional coformer is needed to target optimal sustained drug supersaturation levels. Modulating SA < σ_{crit} and DSP_{index} > 1 allowed for a stable and sustained KTZ release system with supersaturation levels of 6 by 24 h. Findings provide a direct approach for better early decisions regarding cocrystal dose design and/or coformer concentration to be added to formulations to ultimately fine-tune drug supersaturation by coupling dissolution and precipitation processes.

1. Introduction

The design of drug delivery systems that can generate drug supersaturation (σ) in the gastrointestinal tract is considered a viable and well documented strategy to enhance the oral bioavailability of low aqueous soluble drugs. (Sousa et al., 2016; Bhalani et al., 2022; Kuminek et al., 2016) Supersaturation refers to the drug concentration which exceeds its thermodynamic drug solubility. However, a supersaturated state comes with risks due to its thermodynamic instability, which may result in drug precipitation (crystallisation of the most stable drug form) negating the benefits of supersaturation. Strategies to mitigate this risk often rely on the use of formulation additives such as polymers in amorphous solid dispersions (ASD), in which their kinetic behaviour in solution is usually difficult to predict. Unlike cocrystals whereby their mechanistic abilities are easier to predict. (Feng et al., 2021; Kirubakaran et al., 2020).

Cocrystals are one type of supersaturating drug delivery system which possess well-defined stoichiometry and thermodynamic properties which open opportunity for modulating drug solubility and dissolution-pH dependence. (Cao et al., 2019; Chen, 2017; Good & Naír, 2009; Kavanagh et al., 2019) Frequently referred to as incongruently saturating, cocrystals that are more soluble than the parent drug dissociate into their components in solution, followed by drug supersaturation and subsequently drug precipitation. This generates non-stoichiometric solution conditions as the coformer, and drug concentrations do not increase simultaneously. The lifetime of the drug supersaturated state is a result of two competing kinetic processes: cocrystal dissolution and drug precipitation. Dissolution of a cocrystal supplies the solution with drug and precipitation removes it. This behaviour has been described as dissolution-supersaturation-precipitation (DSP) mechanism and has been previously explored for different cocrystal systems. (Machado et al., 2022; Huang et al., 2019; Machado et al., 2020; Mendis & Lakerveld, 2023).

Two metrics can be applied to anticipate and modulate cocrystal DSP: SA and DSP_{index}. Cocrystal solubility (S_{cc}) advantage over drug (SA= S_{cc}/S_{drug}), is an important parameter that represents the theoretical thermodynamic supersaturation limit and the risk for drug precipitation. However, it may not be possible to achieve this theoretical supersaturation in a dissolution vessel. This is because the apparent supersaturation observed during cocrystal in vitro dissolution depends on kinetic parameters, like stirring rate, dose used and more importantly, the drug critical supersaturation, expressed as ($\sigma_{crit} = [D]_n/S_{drug}$). σ_{crit} considers the ratio between critical concentration for drug nucleation ($[D]_n$) and drug equilibrium solubility (S_{drug}) and refers to the supersaturation at which above uncontrolled drug nucleation and

* Corresponding author.
E-mail address: tatiane.machado@newcastle.ac.uk (T.C. Machado).

https://doi.org/10.1016/j.ijpharm.2025.125298
Received 13 December 2024; Received in revised form 17 January 2025; Accepted 27 January 2025
Available online 30 January 2025

growth occur, therefore it represents the kinetic threshold. (Cavanagh et al., 2020) Generating supersaturation closer to this threshold will increase the rate of precipitation. As such, there is a balance between enough supersaturation to provide a solubility advantage over the parent drug against the rate of precipitation, which reduces the lifetime of that supersaturated state. Frequently, cocrystals exhibit unnecessarily high SA, which will increase the risk of drug precipitation. (Huang et al., 2019).

Introduced by Machado et al., the DSP_{index} ($DSP_{index} = C_{dose}/[CF]_{Scc}$) addresses the effects of cocrystal dose (C_{dose}), coformer concentration, and cocrystal solubility on drug supersaturation generated during cocrystal dissolution. DSP_{index} can be applied to determine how non-stoichiometric coformer concentrations can contribute to cocrystal DSP. (Machado et al., 2022).

The influence of non-stoichiometric solution composition on cocrystal solubility can be described by their solubility product (K_{sp}), an equilibrium constant that describes cocrystal equilibrium solubility as a function of its dissolved components (dissolution represented by the left to right arrow and precipitation by the right to left arrow).(Good & Rodríguez-Hornedo, 2009; Nehm et al., 2006) Despite K_{sp} playing a key role in cocrystal development, it is widely overlooked and often misunderstood.

For a binary cocrystal ($Drug_y$ $Coformer_z$), dissolving in an aqueous environment, the equilibrium and associated constant, K_{sp} are:

$$\left(Drug_y Coformer_z\right)_{solid} \overset{K_{sp}}{\rightleftharpoons} y[Drug]_{aq} + z[Coformer]_{aq} \quad (1)$$

where y and z represent the stoichiometric coefficients of the cocrystal components.

For a 1:1 cocrystal, the K_{sp} is given by

$$K_{sp} = [Drug]_0[Coformer]_0 \quad (2)$$

where $[Drug]_0$ $[Coformer]_0$ represent the molar concentration of neutral species of drug and coformer.

K_{sp} can also be expressed in terms of total concentrations (analytical concentrations), $[Drug]_T$ and $[Coformer]_T$ comprising of all drug and coformer species (ionised, solubilised, and complexed components) and is referred to as K_{sp}'$_{total}$.

$$K_{sp'total} = [Drug]_T^y\ [Coformer]_T^z \quad (3)$$

According to the K_{sp}, generation of non-stoichiometric conditions from cocrystal dissolution theoretically reduces cocrystal solubility and subsequently SA. Therefore, the management of DSP behaviour to sustain drug supersaturation can be manipulated by adjusting coformer quantities to alter the cocrystal thermodynamics governed by the K_{sp}. Few studies have previously shown the effect of excess coformer on drug supersaturation generated during cocrystal dissolution.(Kataoka et al., 2023; Yamashita & Sun, 2018) While these studies are interesting, selecting coformer concentrations in an attempt to control DSP behaviour of cocrystals remains a largely empirical and time-consuming process.

We ask, can we make better initial decisions to manage cocrystal DSP by applying a conceptual graphical approach to guide the selection of optimal coformer concentrations? Here, we utilise the theoretical foundation for this approach and shed light on its application with ketoconazole (KTZ) – *p*-aminobenzoic acid (PABA) 1:1 cocrystal, discovered in 2014 by Shayanfar and Jouyban. (Shayanfar & Jouyban, 2014) KTZ-PABA has been studied due to its potential in improving KTZ dissolution and in vivo absorption. (Kataoka et al., 2021). However, there remains a significant research gap in developing approaches to sustain ketoconazole supersaturation generated by cocrystals as well as on formulation development. To apply this approach, we must consider the feasibility for dosage size design and other therapeutic aspects, such as toxicity and clinical application when selecting coformer and cocrystals. Our findings offer pharmaceutical scientists a guide for modulating drug supersaturation from cocrystals systems in a more rational and effective manner, further refining this discovery process over traditional ternary phase diagrams.

2. Materials and methods

2.1. Materials

2.1.1. Cocrystal components

Ketoconazole (KTZ) was purchased from Thermo Scientific Chemicals (Cramlington, UK) and *p*-aminobenzoic acid (PABA) was purchased from Fluorochem (Hadfield, UK). Drug and coformers were characterised by X-ray powder diffraction (XRPD) prior to experiment execution.

2.1.2. Solvents and prepared media

Acetonitrile (ACN) (HPLC grade) and trifluoroacetic acid (analytical grade) were purchased from Thermo Fisher Scientific (Loughborough, UK). Water (HPLC grade) was purchased from Honeywell (Sunderland, UK). Fasted state simulated intestinal fluid (FaSSIF) buffer concentrate and FaSSIF/FeSSIF/FaSSGF 3F powder were acquired from Biorelevant (London, UK). Water used in these studies was filtered through a purification system (Millipore).

2.2. Methods

2.2.1. Cocrystal preparation

Cocrystals were prepared by reaction crystallisation method (RCM) at room temperature. (Rodríguez-Hornedo et al., 2006) The 1:1 KTZ-PABA cocrystal was prepared by adding KTZ to a nearly saturated solution of PABA in ACN. Suspensions were stirred for 24 h and filtered under vacuum. Stoichiometric purity was verified by HPLC, and solid phases were characterised by XRPD and DSC. (see supplementary material Fig. S1-S2) Full conversion to cocrystal was observed within 24 h.

2.2.2. Media preparation

FaSSIF media was prepared by dissolving the appropriate amount of FaSSIF buffer concentrate and FaSSIF/FeSSIF/FaSSGF 3F powder in deionised water, according to manufacturer protocols (Biorelevant.com, Ltd.). The pH of all media used was 6.5. Media were stored at room temperature and used within 48 h of preparation.

2.2.3. Cocrystal and drug solubility measurements

Cocrystal solubility was measured at the eutectic point, in which drug and cocrystal solid phases are in equilibrium with the solution. (Rodríguez-Hornedo et al., 2006) Excess of KTZ and KTZ-PABA were added to 8 mL of FaSSIF media and magnetically stirred at 500 rpm. Suspensions were maintained at 37 °C using a water bath until equilibrium was reached (72–96 h). At 24 h timepoints, 0.8 mL aliquots were taken and filtered via centrifuge through a 0.22 μm cellulose acetate membrane. The pH of each solution was measured, and solid phases were characterised by XRPD to confirm the presence of drug and cocrystal. Filtered solutions were appropriately diluted and analysed by HPLC to determine drug and coformer concentrations. Drug equilibrium solubility was evaluated under same experimental conditions by adding excess drug to 10 mL of FaSSIF media at pH 6.5 until drug solid phase and solution reached equilibrium. Aliquots of 0.8 mL were removed at 24 h timepoints and samples prepared for HPLC analysis as described above to determine drug concentrations.

2.2.4. Graphical approach

The log [Drug] vs log [Coformer] diagram in Fig. 1 was used to evaluate the interplay between cocrystal dissolving constituents, phase stability domains and the driving forces for dissolution and precipitation for the cocrystal studied. It is based on two thermodynamic (S_{cc} and S_{drug}) and one kinetic ($[D]_n$) parameter, and dose to be dissolved,

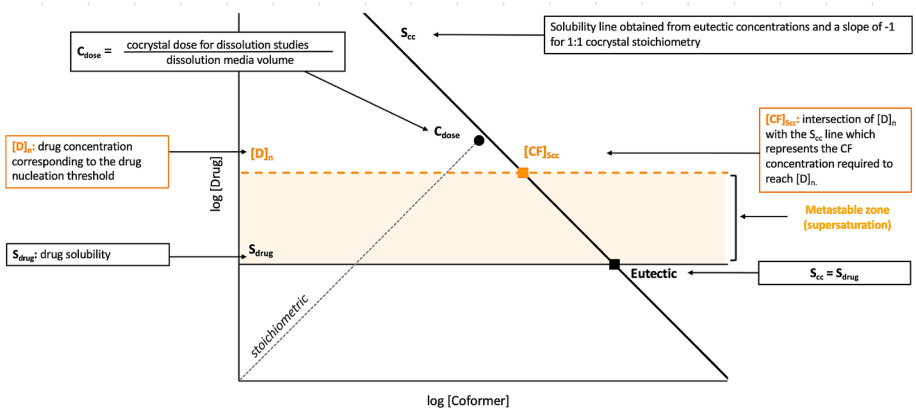

Fig. 1. Schematic diagram depicting the thermodynamic (S_{cc} and S_{drug}) and kinetic ($[D]_n$) parameters. Shaded yellow region displays the region in which supersaturation can be modulated. (For interpretation of the references to colour in this figure legend, the reader is referred to the web version of this article.)

expressed in concentration (C_{dose}).

S_{cc} line has a slope of −1 for a 1:1 cocrystal and was drawn from experimental measurement of the $[Drug]_{eu}$ and $[Coformer]_{eu}$ concentrations at the eutectic point to obtain the K_{sp}'$_{total}$. From the K_{sp}'$_{total}$ Eq. (3), it follows:

$$\log K_{sp}{}'_{total} = \log [Drug] + \log [Coformer] \quad (4)$$

$$\log [Drug] = \log K_{sp}{}'_{total} - \log [Coformer] \quad (5)$$

K_{sp}'$_{total}$ refers to the K_{sp} expressed in terms of total concentrations. S_{drug} = $[Drug]_{eu}$ under the same experimental conditions. S_{cc} and S_{drug} intersect at the eutectic concentrations. The $[D]_n$ refers to the critical concentration for drug nucleation. C_{dose} refers to the mass of cocrystal (mmol) per volume of dissolution media (L) representing the maximum theoretical component concentration, irrespective of solubilities. For a cocrystal with 1:1 stoichiometry, cocrystal dose, drug dose and coformer dose are equal. In this work, the mass of cocrystal used is based on the drug marketed dose of a 200 mg ketoconazole tablet and a luminal volume of 250 mL corresponding to a C_{dose} of 1.51 mM.

This phase diagram shows that non-stoichiometric cocrystal solubility and SA predictably decreases with increase of coformer according to the $K_{sp.}$ Based on this theoretical concept, excess of non-stoichiometric coformer concentrations were applied to modulate cocrystal SA and achieve target supersaturation in different regions of the diagram.

2.2.5. DSP_{index}

To quantify whether coformer concentrations will be adequate to reach cocrystal saturation, we applied the DSP_{index} Eq (6)., previously introduced. (Machado et al., 2022) For pure cocrystal a C_{dose} of 1.51 mM was considered and for all other conditions with additional coformer, the C_{dose} consists of cocrystal dose of 1.51 mM plus the additional PABA concentration added. $[CF]_{Scc}$ is obtained from the intersection of S_{cc} and $[D]_n$ as indicated in Fig. 1.

$$DSP_{index} \overset{def}{=} \frac{C_{dose}}{[CF]_{S_{cc}}} \quad (6)$$

2.2.6. Dissolution studies

Drug and cocrystal powder dissolutions were performed in triplicate in FaSSIF pH 6.5. USP 2 SOTAX dissolution paddle apparatus was used to maintain a temperature of 37 °C and a stirring rate of 150 rpm for up to 24 h. 200 mg of KTZ drug or KTZ-equivalent amount of cocrystal with or without excess PABA was added to 250 mL of FaSSIF media. Prior to analysis KTZ, KTZ-PABA and excess PABA powders were sieved through a 120 μm mesh. For dissolutions performed with additional coformer, the KTZ-PABA and PABA powders were thoroughly mixed before analysis. The pH of FaSSIF media was measured at the beginning and end of each dissolution experiment. Aliquots of 1 mL were taken at predetermined timepoints using a syringe and filtered through a 0.45 μm PES filter. Concentrations of drug and coformer were determined by HPLC and XRPD was used to characterise the final solid phases. The % of cocrystal dissolved at the final timepoint was calculated by considering the cocrystal dose of 1.51 mM as the system is undersaturated with respect to coformer. For dissolutions with additional coformer, it is assumed the PABA added has fully dissolved, and this is confirmed by XRPD (no PABA in the final solid phase).

$$\%\ cocrystal\ dissolved = \frac{moles\ of\ coformer\ dissolved}{initial\ moles\ of\ coformer\ added}\ x\ 100 \quad (7)$$

2.2.7. High performance liquid chromatography (HPLC)

Solution concentrations of drug and coformer were analysed by an Agilent 1260 HPLC instrument equipped with an ultraviolet–visible spectrophotometer detector. A reverse phase Atlantis T3 C18 column (5 μm, 250 x 4.6 mm) maintained at 25 °C ± 0.1 °C was employed. For KTZ-PABA, the mobile phase consisted of ACN and 0.1 %TFA in water using a gradient elution beginning at a 40:60 (ACN:0.1 % TFA in H_2O) to a 60:40 (ACN:0.1 % TFA in H_2O) proportion. A sample injection volume of 5 μL, flow rate of 0.85 mL/min and detector setting of 240 nm for KTZ and PABA detection were employed. Retention times of KTZ and PABA were 5.1 and 3.7 min, respectively.

2.2.8. X-ray powder diffraction (XRPD)

Diffractograms were obtained using a 2Θ x-ray diffractometer in Bragg-Brentano geometry (Malvern Panalytical, UK) operating with a copper Kα radiation (λ = 1.5418 Å), at a current of 40 mA and voltage of 40 kV with a PIXcel 3D detector. The measurements were performed at room temperature, scanning at 2Θ from 5° to 40°, with a 0.0131° step size. Results were compared to diffraction patterns calculated from crystal structures reported in the Cambridge Structural Database (CSD). KTZ-PABA cocrystal CSD identification code is IRIBET. (Groom et al., 2016).

2.2.9. Differential scanning Calorimetry (DSC)

DSC analysis was conducted using a TA DC Q2000 instrument (Cheshire, UK) operating in a temperature range of 25–210 °C. Samples weighing approximately 2 mg were heated at a rate of 10 °C/min under nitrogen gas atmosphere (50 mL/min). Standard aluminium hermetically sealed pans were used for all measurements. The DSC cell was calibrated with indium (T_{peak} = 156 °C; $\Delta H_{fusion\ peak}$ = 28.54 Jg^{-1}). The data obtained were processed using TA instrument software.

3. Results and discussion

3.1. Cocrystal thermodynamic characterisation

To make use of the conceptual diagram in Fig. 1, the first essential step is to evaluate cocrystal equilibrium solubility and its solubility product K_{sp}'$_{total}$. KTZ-PABA equilibrium solubility in FaSSIF was obtained from the measured concentrations of drug and coformer at the eutectic point and represents cocrystal equilibrium solubility under stoichiometric conditions (Table 1). $[KTZ]_{eu} = S_{drug}$ under the studied conditions. Equilibration was observed at pH 5.82 due to PABA self-buffering effect. PABA is an amphoteric compound with $pK_{a1} = 2.41$ and $pK_{a2} = 4.87$. (Lukács et al., 1998) Table 1 also shows predicted thermodynamic parameters at FaSSIF pH 6.5, which correspond to media pH from dissolution studies. Because KTZ is a weak base ($pKa_1 = 3.17$ and $pKa_2 = 6.63$) with pH-dependent solubility, parameters are expected to change as a function of pH. (Avdeef, 2012) KTZ solubility vs pH curve is included in the supplementary material (Fig. S14).

3.2. Defining the metastable zone and the coformer doses for tuning cocrystal DSP

The cocrystal log [KTZ] vs [PABA] diagram in Fig. 2 shows the interplay between dissolved cocrystal constituents, phase stability domains, the driving forces for cocrystal dissolution and KTZ precipitation in FaSSIF pH 6.5. The range between S_{drug} and $[D]_n$ highlighted in yellow is defined as the metastable zone, i.e., a region of drug supersaturation which may not have yet responded to spontaneous nucleation. (Han & Lee, 2017; Kocks et al., 2021) Various studies have reported critical nucleation concentrations for KTZ in FaSSIF, which in terms of supersaturation is approximately $\sigma_{crit} = 16$ (Higashino et al., 2023; Kataoka et al., 2019), which is consistent with our experimental analysis. $\sigma_{crit} = 16$ corresponds to a $[D]_n$ of 0.66 mM in FaSSIF pH 6.5. Above this threshold, KTZ nucleation is expected to be spontaneous. $[D]_n$ is not a constant as it is dependent on multiple factors, such as the dissolution apparatus, pH, stirring rate, media, and temperature. $[D]_n$ is expected to change with pH, while σ_{crit} remains constant. The metastable zone provides a working concentration range in which supersaturation may be generated. (Sun & Lee, 2013).

The selected cocrystal dose (C_{dose}) for dissolution studies shown in the diagram in Fig. 2 refers to the therapeutic KTZ dose of 200 mg and is kept constant across our dissolution studies. Assuming full dose dissolution, C_{dose} does not have the capacity to supply the required component concentrations to reach the $[CF]_{Scc}$, where the cocrystal conversion rates may start decrease. Applying the DSP_{index} (Eq.6), this C_{dose} corresponds to a DSP < 1, therefore, we targeted coformer concentrations to shift the C_{dose} to yield concentrations of PABA closer to $[CF]_{Scc}$ and further, corresponding to a DSP_{index} of ≈1, >1 and ≫1. Selected additional PABA concentrations are 2.59 mM, 5.17 mM, and 10.34 mM.

Table 1
Thermodynamic parameters: S_{cc}, SA and K'_{sptal} obtained from the measured $[KTZ]_{eu,T}$ and $[PABA]_{eu,T}$ at equilibrium with drug and cocrystal solid phases. Equilibrium was achieved between 72 h – 96 h. Predicted data parameters at initial dissolution pH 6.50.

	$[KTZ]_{eu,T}$ (mM)	$[PABA]_{eu,T}$ (mM)	$S_{cc,T}$ (mM)	SA = S_{cc}/ S_{drug}	K'_{sptal} (mM^2)
Experimental value at equilibrium pH 5.82 ± SD	0.089 ± 0.001	11.85 ± 0.11	1.029 ± 0.006[a]	12	1.060 ± 0.012[b]
Predicted value at pH 6.50	0.041	78.098	1.790[c]	44	3.202[d]

[a] $S_{cc,T} = \sqrt{[drug]_{eu,T}[coformer]_{eu,T}}$.
[b] K_{sp}'$_{total}$ experimentally determined from the eutectic concentrations according to K_{sp}'$_{total} = [D]_{T,eu}[CF]_{T,eu}$.
[c] Determined from $S_{cc(FaSSIF)} = S_{cc(aqueous)} \times \sqrt{SP_{drug}}$ ($SP_{drug} = S_{drug\ (FaSSIF)} / S_{drug\ (aqueous)}$).
[d] $K_{sp} = (S_{cc,Fassif})^2$.

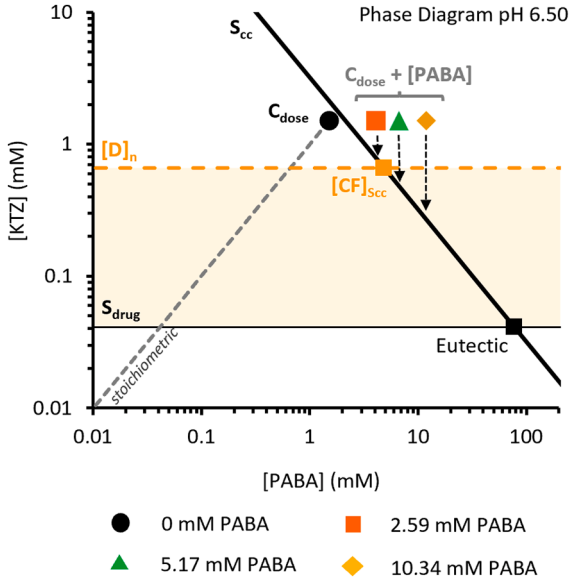

Fig. 2. Phase diagram for KTZ-PABA in FaSSIF pH 6.5 including cocrystal dose (C_{dose}), KTZ-PABA solubility (S_{cc}), KTZ solubility (S_{drug}) and critical concentration ($[D]_n$). $[D]_n$ corresponds to the KTZ nucleation threshold at $\sigma_{crit} = 16$. The S_{cc} line was drawn from the predicted data at pH 6.5 (Table 1). $[CF]_{Scc}$ is the coformer concentration at the cocrystal solubility line at the intersection with $[D]_n$. For KTZ-PABA the C_{dose} does not supply $[CF]_{Scc}$. Additional coformer concentrations selected for analysis are depicted by symbols and correspond to C_{dose} (1.51 mM) + PABA concentrations indicated.

3.3. Cocrystal DSP pathways and drug vs coformer phase diagrams

KTZ vs time profiles from KTZ-PABA dissolutions in FaSSIF as a function of different non-stoichiometric concentrations of PABA are shown in Fig. 3. Graphs on the right show dissolved component concentrations expressed into the phase diagram to allow for kinetic and thermodynamic correlations. With the purpose to establish a more accurate relationship, all elements of the diagram correspond to the final dissolution pH. A pH range of 5.7–6.6 was observed in these dissolution studies which may reflect on S_{drug} changes from 0.112 to 0.041 mM, respectively (Fig. S14). This notable change in solubility emphasises the influence pH has on KTZ solubility, $[D]_n$ and consequently on cocrystal DSP. The equation to predict KTZ solubility as a function of pH and micellar solubilisation is included in the supplementary material (Fig. S14). Pure KTZ dissolution can be found in the supplementary material (Fig. S4).

Dissolution of KTZ-PABA (251.6 mg in 250 mL) corresponding to a C_{dose} of 1.51 mM, exhibited a typical DSP profile: initial spike of drug, reaching a $C_{max} = 0.667 \pm 0.002$ mM in 15 min followed by solution mediated transformation of cocrystal to the less soluble KTZ form (Fig. 3A). PABA concentration increases due to cocrystal incongruent saturation behaviour, deviating from the 1:1 stoichiometric line as drug concentrations approach $[D]_n$ (where KTZ nucleation occurs). KTZ-PABA dissolution with the lowest additional coformer concentration (2.59 mM) in Fig. 3, resulted in similar cocrystal DSP profile to KTZ-PABA pure dissolution in Fig. 3A ($p \geq 0.05$). It shows a $C_{max} = 0.648 \pm 0.008$ mM followed by cocrystal transformation to drug. (Table 2) Full cocrystal dissolution was confirmed by the presence of KTZ in the final dissolution solid phase (Fig. S7). With the addition of 5.17 mM PABA, cocrystal dissolution exhibited a controlled DSP profile where KTZ achieved a $C_{max} = 0.347 \pm 0.017$ mM at 15 min which was sustained for

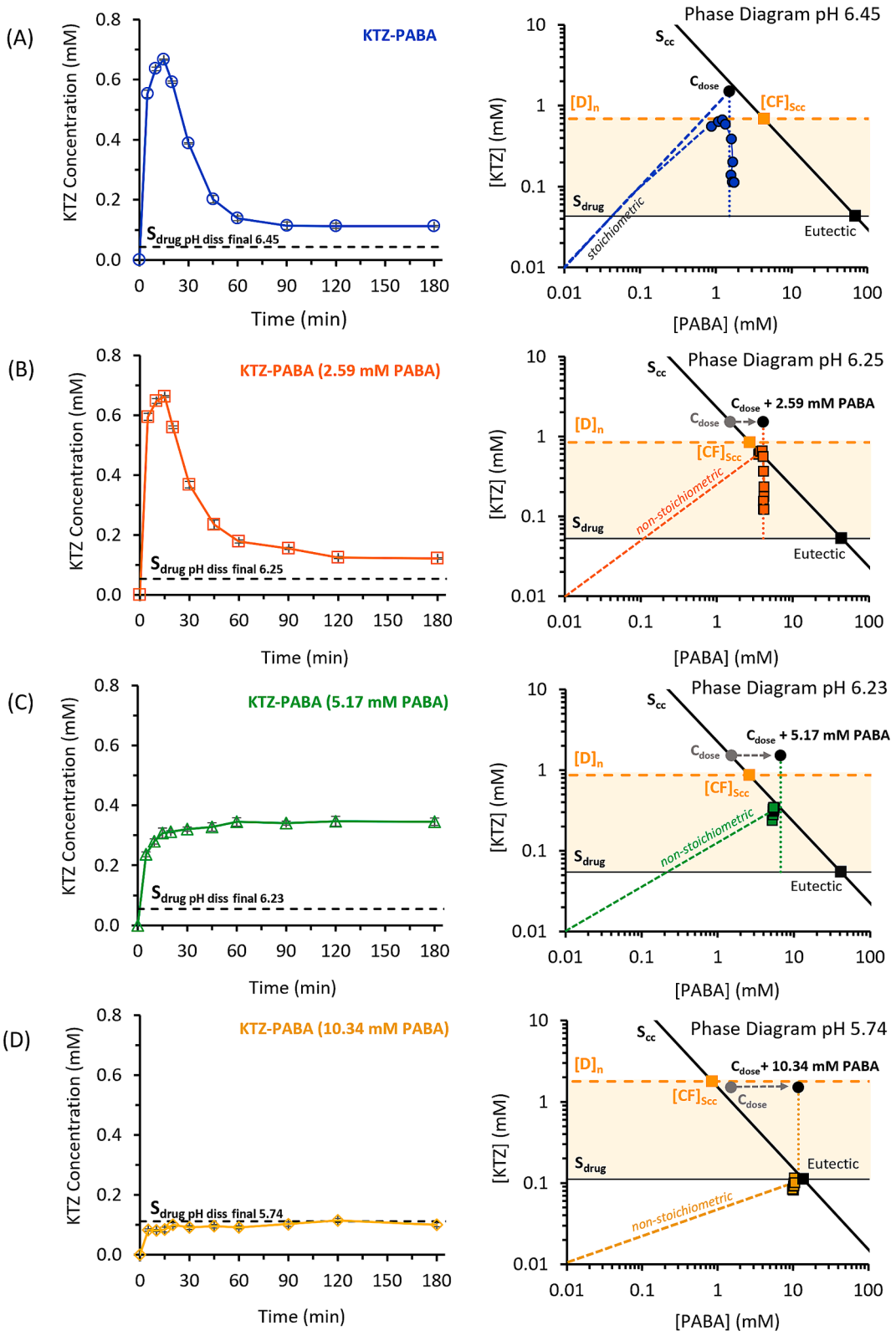

Fig. 3. Drug concentration vs time dissolution profiles during KTZ-PABA dissolution with (A) 0 mM PABA, (B) 2.59 mM PABA, (C) 5.17 mM PABA and (D) 10.34 mM PABA in FaSSIF pH 6.5 (0–180 min). Graphs in the right show drug and coformer concentrations during cocrystal dissolution studies in the context of the phase diagram. S_{cc}, S_{drug} and $[D]_n$ at final dissolution pH is depicted in each profile. C_{dose} indicates cocrystal dose of 1.51 mM and grey dashed arrow shows shift with additional PABA. Theoretical stoichiometric and non-stoichiometric dashed lines are displayed in each diagram to represent dissolution between 0–5 min. Cocrystal dissolution driving force is reduced as coformer concentrations approaches cocrystal solubility line below the $[D]_n$.

Table 2
Dissolution key parameters for pure KTZ and for KTZ-PABA with and without excess PABA, which concentration values are in parenthesis. Initial dissolution pH = 6.5.

Solid form	C_{max} (mM) ± SD	T_{max} (min)	AUC $_{0\text{-}180min}$ (mM.min) ± SD	Final solid form[a,b]	Final dissolution pH[a] ± SD
KTZ	0.046 ± 0.002	90	7.47 ± 0.46	KTZ	6.57 ± 0.01
KTZ-PABA (0 mM)	0.667 ± 0.002	15	34.62 ± 3.54	KTZ	6.45 ± 0.01
KTZ-PABA (2.54 mM)	0.648 ± 0.008	15	39.68 ± 0.38	KTZ	6.25 ± 0.01
KTZ-PABA (5.17 mM)	0.347 ± 0.017	120	59.31 ± 1.92	KTZ-PABA	6.22 ± 0.02
KTZ-PABA (10.34 mM)	0.116 ± 0.006	120	17.95 ± 0.41	KTZ-PABA	5.74 ± 0.01

[a] Final refers to 180-min time point.
[b] Characterised by XRPD.

the duration of the experiment (180 min). The additional PABA generated non-stoichiometric solution conditions that supplies coformer saturation at S_{cc} line in a region below $[D]_n$, where the thermodynamic drive for drug precipitation is lower. The mechanism behind this behaviour is that the cocrystal dissolution temporarily freezes until more drug precipitates and cocrystal dissolution can resume. Based on the meaning of K_{sp} one expects that increasing the coformer concentrations will predictably decrease cocrystal solubility, as long as there are no other solution molecular interactions, such as complexation. A phase solubility study was conducted and confirmed no complexation between KTZ and PABA. (Fig.S13) The final solid phase of cocrystal dissolution with additional 5.17 mM PABA is KTZ-PABA according to XRPD analysis (Fig. S8). By the end of experiment only 14.8 % of cocrystal was dissolved.

The attempt to show how the cocrystal performs with higher PABA concentrations (10.34 mM) resulted in no supersaturation, with KTZ reaching its thermodynamic solubility in 120 min, limiting further dissolution. (Fig. 3D) The final solid phase at the end of dissolution was identified as cocrystal, with 14.3 % of cocrystal dissolved by 180 min (Fig. S9). This finding shows that by providing a dose that can supply the coformer eutectic concentrations, the system is directed to a region of thermodynamic stability, ultimately negating the cocrystal solubility advantage, as $S_{cc} = S_{drug}$. Therefore, cocrystal cannot further dissolve as the drug is not precipitating. The addition of 10.34 mM PABA with a cocrystal C_{dose} of 1.51 mM supplies the $[PABA]_{eu}$ of 11.85 mM (Table 1).

3.4. Supersaturation vs time profiles correlated with DSP_{index} and SA

The cocrystal SA values for each dissolution condition shown in Fig. 4B and Table 3 were obtained from the S_{cc} to S_{drug} ratio, considering $S_{cc} = K_{sp}'_{total}/[PABA]_{added}$. They represent the theoretical thermodynamic limit of supersaturation in the dissolution conditions studied (FaSSIF, final dissolution pH and excess PABA concentration). KTZ-PABA solubility corresponds to a SA = 46 at dissolution conditions without excess PABA, which is higher than the $\sigma_{crit} = 16$. This unnecessarily high SA, allows the critical supersaturation limit to be quickly approached as shown in Fig. 4A, promoting rapid drug precipitation at 15 min. In the presence of excess coformer, the SA is known to predictably decrease as per the definition of $K_{sp.}$ Thus, the addition of 2.59 mM corresponds to a theoretical SA = 17 which still above the σ_{crit}. In both cases, σ_{crit} is limiting KTZ supersaturation generated during dissolution.

In contrast, the dissolution of cocrystal dose with additional 10.34 mM PABA, generated solution conditions close to eutectic point, where cocrystal solubility advantage is negated, i.e. SA = 1. Cocrystals dissolves stoichiometrically with respect to its constituents with no drug supersaturation. When SA is modulated below the σ_{crit}, the risk of drug precipitation can be mitigated. This was previously shown by Cavanagh et al., in a study with danazol cocrystals whereby additives modulated cocrystal SA below danazol σ_{crit}, generating a sustained supersaturation during cocrystal dissolution. (Cavanagh et al., 2020) This is consistent with our results where the addition of 5.17 mM PABA modulated the theoretical SA to 8 which is below $\sigma_{crit} = 16$, therefore cocrystal dissolution is limited by its solubility and not the σ_{crit}.

In context of DSP_{index}, pure KTZ-PABA dose dissolution corresponds to a $DSP_{index} = 0.35$, which means that the dose does not supply the required coformer concentrations to reach $[CF]_{Scc}$. This can be seen in Fig. 3A. The addition of coformer allowed for a shift in C_{dose}, increasing the DSP_{index} to values of 1.5, 2.6 and 13.9 (Table 3). When $DSP_{index} > 1$, the dose is enough to supply $[CF]_{Scc}$ at σ_{crit}. As dissolution concentrations approach S_{cc} at this point, the driving forces for cocrystal

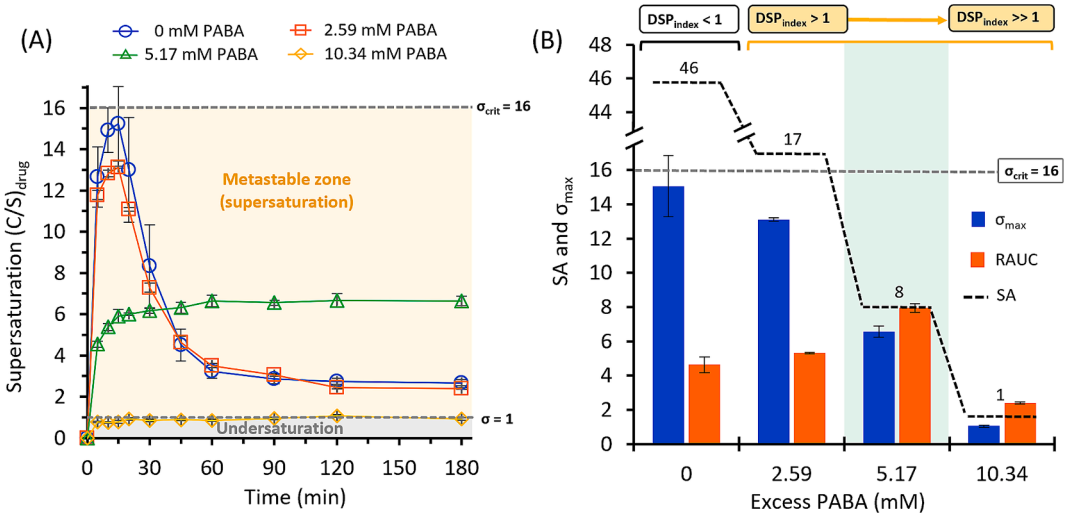

Fig. 4. (A) Drug supersaturation vs time profiles during cocrystal dissolution with and without excess PABA. Supersaturation and under supersaturation zones and the σ_{crit} included for visualisation. (B) SA, σ_{max} and RAUC for KTZ-PABA cocrystal with and without excess PABA (0–180 min). Numbers following dashed line refers to the SA. The DSP_{index} shown above diagram for each condition studied. A short-lived supersaturation is expected when SA > σ_{crit}. Shaded results for 5.17 mM PABA depict the optimal outcome, which resulted in highest observed RAUC = 8.

Table 3
Summary of dissolution metrics including SA, DSP_{index} and key dissolution parameters, σ_{max} and RAUC.

KTZ-PABA ($PABA_{added}$)	SA	σ_{max} [a] ± SD	RAUC $_{0\text{-}180min}$ [b] ± SD	$[D]_n$ (mM)[c]	$[CF]_{Scc} = K_{sp}{}^{*}{}_{total}/[D]_n$ (mM)	$[PABA]_{total}$ (mM)[d]	DSP_{index}
(0 mM)	46	15.1 ± 1.8	4.63 ± 0.47	0.689	4.341	1.51	0.35[e]
(2.59 mM)	17	13.1 ± 0.1	5.31 ± 0.05	0.846	2.733	4.10	1.50[f]
(5.17 mM)	8	6.6 ± 0.3	7.94 ± 0.26	0.870	2.587	6.68	2.58[f]
(10.34 mM)	1	1.0 ± 0.1	2.40 ± 0.06	1.790	0.850	11.85	13.94[f]

[a] Maximum supersaturation ($\sigma_{max=}$ C_{max}/S_{drug}).
[b] RAUC = $AUC_{cocrystal}$ /AUC_{drug}.
[c] Determined considering a σ_{crit} = 16.
[d] $[PABA]_{total}$ = C_{dose} + $[PABA]_{added}$
[e] DSP_{index}= C_{dose} / $[CF]_{Scc}$.
[f] DSP_{index} = $[PABA]_{total}$ / $[CF]_{Scc}$.

dissolution and drug precipitation are expected to slow, initiating a steady state. Our findings with KTZ show that targeting a zone nearby σ_{crit} remains a risk due to the high driving force for drug precipitation. As observed in the dissolution with 5.17 mM PABA, when SA is modulated units below the σ_{crit} (8 vs 16) the driving forces for cocrystal dissolution and drug precipitation reduced, coupling the two processes, and generating sustained supersaturation.

These trends are best appreciated by analysing Fig. 4B, which compares the observed supersaturation, relative area under the curve (RAUC = $AUC_{cocrystal}$ /AUC_{drug}), SA and the DSP_{index}. Optimal sustained supersaturation is emphasised by an 8-fold increase in KTZ AUC.

3.5. Supersaturation over a 24-hr period

With the purpose of evaluating the duration of sustained supersaturation shown in the 3 h dissolution with 5.17 mM PABA, we extended analysis time to 24 h. Fig. 5A shows KTZ sustained σ = 4.7–6.3 for the duration of the experiment with very low de-supersaturation rates. A decrease in KTZ supersaturation between the 3 and 24 h timepoint was deemed statistically significant ($p < 0.05$). At 24 h, 41.7 % of cocrystal dose was dissolved, in comparison to the 3 h dissolution in which 14.8 % of cocrystal was dissolved at the final time point. Final solid phase analysis by XRPD was identified as cocrystal however, DSC detected the presence of KTZ, which is consistent as solution mediated transformation is occurring (Fig. S11-S12). KTZ may not be detected by XRPD due the lack of sensitivity for small KTZ traces.

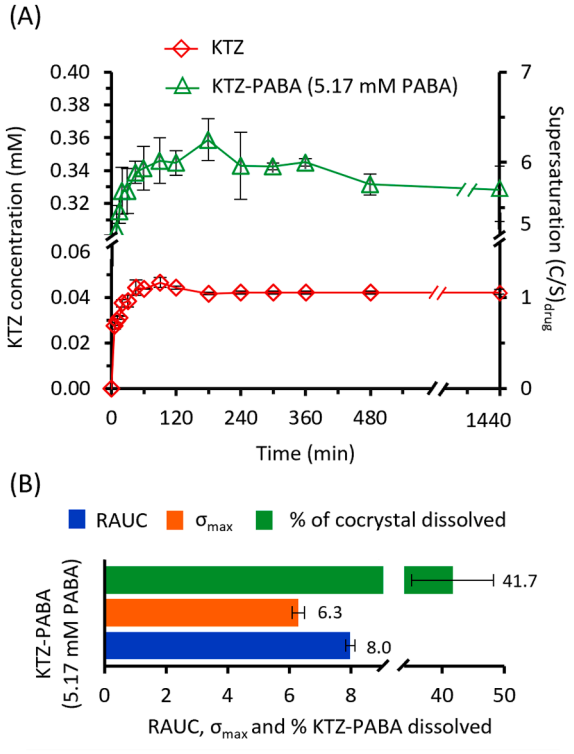

Fig. 5. (A) Drug supersaturation and concentration vs time profile during KTZ-PABA cocrystal dissolution with 5.17 mM excess PABA in pH 6.5 FaSSIF (0–24 h). Cocrystal final dissolution pH 6.18 ± 0.01. Dissolution profile of pure KTZ has been extrapolated from 3 to 24 h for comparison. (B) RAUC, σ_{max} and % of cocrystal dissolved for KTZ-PABA cocrystal with 5.17 mM excess PABA in the dissolution media studied (0–24 h). Errors bars indicate standard deviation.

Cocrystal to drug dissolution comparison in Table 4 shows a significant increase in AUC (0–24 h) 475.09 $mM.min^{-1}$ vs 59.56 $mM.min^{-1}$, respectively, corresponding to an 8-fold increase in AUC compared to the drug. These findings demonstrate the power of this approach in synchronising cocrystal dissolution and drug precipitation processes, allowing for high drug concentrations to be sustained longer. From the 24 h analysis, we emphasise a controlled supersaturating system with a remaining 58.3 % of cocrystal dose still to dissolve. (Fig. 5B).

A study by Amponsah-Efah et al., with KTZ-polymer ASD's generated sustained supersaturation levels around 6 by the end of the 2.5 h study. (Amponsah-Efah et al., 2021) These results are close to the σ_{max} we obtained in our study with 5.17 mM PABA however, we have been able to sustain supersaturation for an extended lifetime without the use of polymers. Furthermore, polymer selection for ASD's is usually done empirically which is often time consuming and costly. In contrast, our approach employs a mechanistic understanding of cocrystal DSP with minimal experimental exploration. By targeting coformer concentrations for control of DSP behaviour, we can initiate a supersaturation with the ability to be sustained.

Lack of understanding of solution behaviour of supersaturation states results in trial-and-error approaches which can prove to be a costly and time-consuming processes. The target coformer concentrations tested in this work are practical concentrations that could be added as part of a cocrystal dosage form. The use of the conceptual diagram and the DSP_{index} allows for rational coformer concentration selection which is feasible for the stage of pre-formulations and formulation.

4. Conclusion

We have shown that is possible to significantly extend drug supersaturation generated during cocrystal dissolution by modulating drug concentrations below their critical supersaturation (σ_{crit}). By integrating two thermodynamic parameters (S_{cc} and S_{drug}) and one kinetic parameter (σ_{crit}) into a conceptual diagram previously introduced (Machado et al., 2022), we can predict dissolution behaviour for a given cocrystal dose. Our results suggest that this approach can be applied to other solid systems with well-defined stoichiometry where an extended drug release profile is desired. Additionally, the use polymers or other additives such as lipids, can be considered in formulations, to further optimize drug release behaviour. We are interested in exploring this behaviour in vivo where dynamic effects such as absorption could influence the cocrystal DSP profile.

Table 4
Dissolution key parameters for 0–24 h dissolution with 5.17 mM excess PABA. KTZ extrapolated data from 0-3 h dissolution included for comparison.

Solid form	C_{max} (mM) ± SD	T_{max} (mM) ± SD	$AUC_{0\text{-}24h}$ (mM.min^{-1}) ± SD	$RAUC_{0\text{-}24h}$ [a] ± SD	σ_{max} [b] ± SD	Final % of cocrystal dissolved[c] ± SD	Final solid phase[c,d]
KTZ	0.046 ± 0.002	90	59.56 ± 1.00	–	–	–	KTZ
KTZ-PABA (5.17 mM PABA)	0.359 ± 0.013	180	475.09 ± 8.20	7.98 ± 0.15	6.3 ± 0.2	41.7 ± 6.6	KTZ-PABA

[a] RAUC = $AUC_{\text{drug concentration during drug dissolution}}/AUC_{\text{drug concentration from cocrystal dissolution}}$
[b] Maximum supersaturation ($\sigma_{max=}$ C_{max}/S_{drug}).
[c] Final refers to 24 h timepoint.
[d] Characterised by XRPD.

CRediT authorship contribution statement

Lucy M. Newman: Writing – review & editing, Writing – original draft, Visualization, Methodology, Investigation, Formal analysis. **Oisín N. Kavanagh:** Writing – review & editing, Formal analysis, Conceptualization. **Tatiane C. Machado:** Writing – review & editing, Supervision, Project administration, Methodology, Formal analysis, Conceptualization.

Declaration of competing interest

The authors declare that they have no known competing financial interests or personal relationships that could have appeared to influence the work reported in this paper.

Acknowledgments

The authors gratefully acknowledge the Engineering and Physical Sciences Research Council (EPSRC) for the funding of this PhD studentship (EP/W524700/1) and Professor Emerita Naír Rodriguez-Hornedo (University of Michigan) for valuable discussions. Oisín Kavanagh is funded by Action Medical Research/LifeArc grant (GN3039) and an EPSRC New Investigator award (EP/Y014596/1).

Appendix A. Supplementary material

Supplementary data to this article can be found online at https://doi.org/10.1016/j.ijpharm.2025.125298.

Data availability

Data will be made available on request.

References

Amponsah-Efah, K.K., Mistry, P., Eisenhart, R., Suryanarayanan, R., 2021. The influence of the strength of drug-polymer interactions on the dissolution of amorphous solid dispersions. *Mol. Pharm.* 18 (1), 174–186. https://doi.org/10.1021/acs.molpharmaceut.0c00790.

Avdeef, Alex, 2012. Absorption and Drug Development (Second). John Wiley & Sons. Doi: 10.1002/9781118286067.

Bhalani, D.V., Nutan, B, Kumar, A., Singh Chandel, A.K., 2022. Bioavailability enhancement techniques for poorly aqueous soluble drugs and therapeutics. *Biomedicines* 10 (9), 2055. https://doi.org/10.3390/biomedicines10092055.

Cao, F., Rodriguez-Hornedo, N., Amidon, G.E., 2019. Mechanistic Analysis of cocrystal dissolution, surface pH, and dissolution advantage as a guide for rational selection. *J. Pharm. Sci.* 108 (1), 243–251. https://doi.org/10.1016/j.xphs.2018.09.028.

Cavanagh, K. L., Kuminek G. , Rodríguez-Hornedo N. Cocrystal Solubility Advantage and Dose/Solubility Ratio Diagrams: A Mechanistic Approach To Selecting Additives and Controlling Dissolution-Supersaturation-Precipitation Behavior. Mol Pharm. 2020 Nov 2;17(11):4286-4301. doi: 10.1021/acs.molpharmaceut.0c00713. Epub 2020 Oct 19. PMID: 32815731.

Chen, Y.M., 2017. *Cocrystals Mitigate the Effect of pH on Solubility and Dissolution of Basic Drugs*. University of Michigan.

Feng, Y., Meng, Y., Tan, F., Lv, L., Li, Z., Wang, Y., Yang, Y., Gong, W., Yang, M., 2021. Effect of surfactants and polymers on the dissolution behavior of supersaturable tecovirimat-4-hydroxybenzoic acid cocrystals. *Pharmaceutics* 13 (11). https://doi.org/10.3390/pharmaceutics13111772.

Good, D.J., Naír, R.H., 2009. Solubility advantage of pharmaceutical cocrystals. *Cryst. Growth Des.* 9 (5), 2252–2264. https://doi.org/10.1021/cg801039j.

Good, D.J., Rodríguez-Hornedo, N., 2009. Solubility advantage of pharmaceutical cocrystals. *Cryst. Growth Des.* 9, 2253–2264. https://doi.org/10.1021/cg801039j.

Groom, C.R., Bruno, I.J., Lightfoot, M.P., Ward, S.C., 2016. *The Cambridge structural database*. CSD. https://doi.org/10.1107/S2052520616003954.

Han, Y.R., Lee, P.I., 2017. Effect of extent of supersaturation on the evolution of kinetic solubility profiles. *Mol. Pharm.* 14 (1), 206–220. https://doi.org/10.1021/acs.molpharmaceut.6b00788.

Higashino, H., Minami, K., Takagi, T., Kataoka, M., Yamashita, S., 2023. The effects of degree and duration of supersaturation on in vivo absorption profiles for highly permeable drugs, dipyridamole and ketoconazole. *Eur. J. Pharm. Biopharm.* 189 (June), 48–55. https://doi.org/10.1016/j.ejpb.2023.06.002.

Huang, Y., Kuminek, G., Roy, L., Cavanagh, K.L., Yin, Q., Rodríguez-Hornedo, N., 2019. Cocrystal solubility advantage diagrams as a means to control dissolution, supersaturation, and precipitation. *Mol. Pharm.* 16 (9), 3887–3895. https://doi.org/10.1021/acs.molpharmaceut.9b00501.

Kataoka, M., Takeyama, S., Minami, K., Higashino, H., Kakimi, K., Fujii, Y., Takahashi, M., Yamashita, S., 2019. In vitro assessment of supersaturation/precipitation and biological membrane permeation of poorly water-soluble drugs: a case study with albendazole and ketoconazole. *J. Pharm. Sci.* 108 (8), 2580–2587. https://doi.org/10.1016/j.xphs.2019.03.007.

Kataoka M, Minami K, Takagi T, Amidon GE, Yamashita S. In Vitro-In Vivo Correlation in Cocrystal Dissolution: Consideration of Drug Release Profiles Based on Coformer Dissolution and Absorption Behavior. Mol Pharm. 2021 Nov 1;18(11):4122-4130. doi: 10.1021/acs.molpharmaceut.1c00537. Epub 2021 Oct 7. PMID: 34618448.

Kataoka, M., Yonehara, A., Minami, K., Takagi, T., Yamashita, S., 2023. Control of dissolution and supersaturation/precipitation of poorly water-soluble drugs from cocrystals based on solubility products: a case study with a ketoconazole cocrystal. *Mol. Pharm.* 20 (8), 4100–4107. https://doi.org/10.1021/acs.molpharmaceut.3c00237.

Kavanagh, O.N., Croker, D.M., Walker, G.M., Zaworotko, M.J., 2019. Pharmaceutical cocrystals: from serendipity to design to application. *Drug Discov. Today* 24 (3), 796–804. https://doi.org/10.1016/j.drudis.2018.11.023.

Kirubakaran, P., Wang, K., Rosbottom, I., Cross, R.B.M., Li, M., 2020. Understanding the effects of a polymer on the surface dissolution of pharmaceutical cocrystals using combined experimental and molecular dynamics simulation approaches. *Mol. Pharm.* 17 (2), 517–529. https://doi.org/10.1021/acs.molpharmaceut.9b00955.

Kocks, C., Krekel, C.M., Gausmann, M., Jupke, A., 2021. Determination of the metastable zone width and nucleation parameters of succinic acid for electrochemically induced crystallization. *Crystals* 11 (9). https://doi.org/10.3390/cryst11091090.

Kuminek, G., Cao, F., de Oliveira, B., da Rocha, A., Gonçalves Cardoso, S., Rodríguez-Hornedo, N., 2016. Cocrystals to facilitate delivery of poorly soluble compounds beyond-rule-of-5. *Adv. Drug Deliv. Rev.* 101, 143–166. https://doi.org/10.1016/j.addr.2016.04.022.

Lukács, M., Barcsa, G., Kovács-Hadady, K., 1998. The effects of pH, ionic strength and buffer concentration of mobile phase on RF of acidic compounds in ion-pair TLC. *Chromatographia* 48, 511516. https://doi.org/10.1007/BF02466642.

Machado, T.C., Kuminek, G., Cardoso, S.G., Rodríguez-Hornedo, N., 2020. The role of pH and dose/solubility ratio on cocrystal dissolution, drug supersaturation and precipitation. *Eur. J. Pharm. Sci.* 152 (June), 105422. https://doi.org/10.1016/j.ejps.2020.105422.

Machado, T.C., Kavanagh, O.N., Cardoso, S.G., Rodríguez-Hornedo, N., 2022. Synchronization of cocrystal dissolution and drug precipitation to sustain drug supersaturation. *Mol. Pharm.* 19 (8), 2765–2775. https://doi.org/10.1021/acs.molpharmaceut.2c00122.

Mendis, N.P., Lakerveld, R., 2023. An in vitro model for cocrystal dissolution with simultaneous surface and bulk precipitation. *Mol. Pharm.* 20 (11), 5486–5499. https://doi.org/10.1021/acs.molpharmaceut.3c00334.

Nehm, S.J., Rodríguez-Spong, B., Rodríguez-Hornedo, N., 2006. Phase solubility diagrams of cocrystals are explained by solubility product and solution complexation. *Cryst. Growth Des.* 6 (2), 592–600. https://doi.org/10.1021/cg0503346.

Rodríguez-Hornedo N, Nehm SJ, Seefeldt KF, Pagan-Torres Y, Falkiewicz CJ. Reaction crystallization of pharmaceutical molecular complexes. Mol Pharm. 2006 May-Jun;3(3):362-7. doi: 10.1021/mp050099m. PMID: 16749868.

Shayanfar, A., Jouyban, A., 2014. Physicochemical characterization of a new cocrystal of ketoconazole. *Powder Technol.* 262, 242–248. https://doi.org/10.1016/j.powtec.2014.04.072.

Sousa, L.A., Reutzel-Edens, S.M., Stephenson, G.A., Taylor, L.S., 2016. Supersaturation Potential of Salt, Co-Crystal, and Amorphous Forms of a Model Weak Base. Crystal Growth & Design 16, 737–748.

Sun, D.D., Lee, P.I., 2013. Evolution of supersaturation of amorphous pharmaceuticals: the effect of rate of supersaturation generation. *Mol. Pharm.* 10 (11), 4330–4346. https://doi.org/10.1021/mp400439q.

Yamashita, H., Sun, C.C., 2018. Improving dissolution rate of carbamazepine-glutaric acid cocrystal through solubilization by excess coformer. *Pharm. Res.* 35 (1). https://doi.org/10.1007/s11095-017-2309-x.